ADVANCES IN ATMOSPHERIC SCIENCES, VOL. 33, JUNE 2016, 695–705

# Simple Metrics for Representing East Asian Winter Monsoon Variability: Urals Blocking and Western Pacific Teleconnection Patterns

Hoffman H. N. CHEUNG[1,2] and Wen ZHOU*[1,2]

[1] *Guy Carpenter Asia-Pacific Climate Impact Centre, School of Energy and Environment, City University of Hong Kong, Hong Kong SAR*

[2] *City University of Hong Kong Shenzhen Research Institute, Shenzhen* 518057

(Received 18 September 2015; revised 11 November 2015; accepted 30 November 2015)

ABSTRACT

Instead of conventional East Asian winter monsoon indices (EAWMIs), we simply use two large-scale teleconnection patterns to represent long-term variations in the EAWM. First, the Urals blocking pattern index (UBI) is closely related to cold air advection from the high latitudes towards western Siberia, such that it shows an implicit linkage with the Siberian high intensity and the surface air temperature (SAT) variations north of 40°N in the EAWM region. Second, the well-known western Pacific teleconnection index (WPI) is connected with the meridional displacement of the East Asian jet stream and the East Asian trough. This is strongly related to the SAT variations in the coastal area south of 40°N in the EAWM region. The temperature variation in the EAWM region is also represented by the two dominant temperature modes, which are called the northern temperature mode (NTM) and the southern temperature mode (STM). Compared to 19 existing EAWMIs and other well-known teleconnection patterns, the UBI shows the strongest correlation with the NTM, while the WPI shows an equally strong correlation with the STM as four EAWMIs. The UBI–NTM and WPI–STM relationships are robust when the correlation analysis is repeated by (1) the 31-year running correlation and (2) the 8-year high-pass and low-pass filter. Hence, these results are useful for analyzing the large-scale teleconnections of the EAWM and for evaluating this issue in climate models. In particular, more studies should focus on the teleconnection patterns over extratropical Eurasia.

**Key words**: East Asian winter monsoon, Urals blocking high, western Pacific teleconnection pattern, teleconnection

**Citation**: Cheung, H. H. N., and W. Zhou, 2016: Simple metrics for representing East Asian winter monsoon variability: Urals blocking and western Pacific teleconnection patterns. *Adv. Atmos. Sci.*, **33**(6), 695–705, doi: 10.1007/s00376-015-5204-6.

## 1. Introduction

The intensity of the East Asian winter monsoon (EAWM) is closely related to severe conditions in densely populated regions in East Asia, including China, Japan, and Korea. A simple and predictable EAWM index (EAWMI) is important for seasonal forecasting and for studying the long-term variations of the EAWM. Based on large-scale circulation features over the EAWM region (Fig. 1), many previous works have constructed different EAWMIs using: (1) the mean SLP (MSLP) gradient between East Asia and the Pacific Ocean; (2) the lower tropospheric wind along the coastal region of East Asia; (3) the East Asian trough; and (4) the upper tropospheric zonal wind shear (Wang and Chen, 2010). Yet, the EAWM is a complicated system involving the air–sea interaction between the Asian continent and the Pacific Ocean, and the topographic forcing exerted by the Tibetan Plateau. The interannual variations of surface air temperature (SAT) in the northern and southern parts of the EAWM region are uncorrelated (Wang et al., 2010a). Therefore, it is challenging to construct a unified index that can successfully capture the SAT variations in the entire EAWM region.

The evolution of the EAWM system is related to middle and upper tropospheric remote signals from both upstream and downstream (e.g., Chang and Lau, 1980; Joung and Hitchman, 1982; Lau and Lau, 1984; Hsu and Wallace, 1985; Takaya and Nakamura, 2005, 2013; Song et al., 2014). A typical severe cold-air outbreak in the EAWM region is characterized by an inverted-omega geopotential height pattern. This is composed of two blocking ridges over the Urals–Siberia region and the North Pacific (Yeh et al., 1962; Ding, 1994). A recent study by Cheung et al. (2015) showed that the long-term variation in the number of cold days (not the year-to-year SAT variability) in Hong Kong, a coastal city in Southeast China, is closely related to the frequency of the Urals blocking pattern index (UBI) and the western Pacific teleconnection pattern index (WPI). In this paper, we will further show how both the UBI and WPI constitute one of the most robust signals accounting for the year-to-year

* Corresponding author: Wen ZHOU
Email: wenzhou@cityu.edu.hk

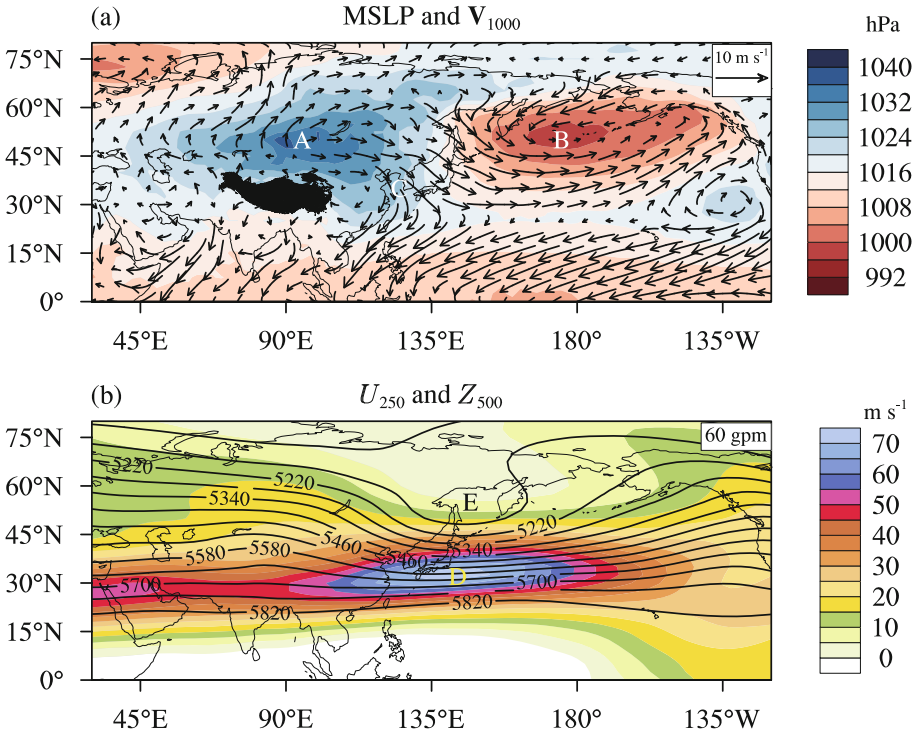


**Fig. 1.** Large-scale circulation features of the EAWM: (a) MSLP (shading; units: hPa) and the 1000-hPa wind (vectors; units: m $s^{-1}$); and (b) $U_{250}$ (shading; units: m $s^{-1}$) and $Z_{500}$ (contour interval: 60 gpm). In (a), the Tibetan Plateau is colored black, while A, B and C denote the Siberian high, Aleutian low and near-surface northeasterly flow over the East Asian coast, respectively. In (b), D and E denote the East Asian jet stream and East Asian trough, respectively.

SAT variability in the EAWM region. Unlike most previous works, which tended to focus on the relationship between blocking/teleconnections and EAWM variability (Gong et al., 2001; Lee and Jhun, 2006; Liu et al., 2014; Lim and Kim, 2015), our analysis begins with the SAT in the EAWM region.

Following the definition of Wang et al. (2010a), the SAT variation in the EAWM region will also be described by the two major temperature modes. The northern temperature mode (NTM) captures the temperature variation north of 40°N well, whereas the southern temperature mode (STM) successfully depicts the temperature variation south of 40°N. Compared to 19 EAWMIs and other well-known teleconnection indices, we will demonstrate that the UBI shows the strongest correlation with the NTM, which is poorly captured by most of the EAWMIs. The WPI shows an equally strong correlation with the STM with four EAWMIs. Because the UBI–NTM and WPI–STM correlations exceed 0.7 in magnitude on both interannual and interdecadal timescales, we suggest that Urals blocking (UB) and western Pacific (WP) teleconnection are crucial for EAWM studies. Based on the findings of this study and other recent studies, we will also discuss the key to defining a representative EAWMI.

The present study investigates 66 winters, from 1948/49 to 2013/14, using the NCEP–NCAR reanalysis datasets. These include the daily field of geopotential height ($Z$), the monthly field of SAT, MSLP, and the zonal and meridional components of wind ($U$ and $V$). Following this introduction, the teleconnection indices (UBI and WPI) are defined in section 2. Section 3 presents the relationship between these teleconnection indices and the temperature variations in the EAWM region. Section 4 highlights the strength of these teleconnection indices to represent the EAWM variability. The results are summarized and discussed in section 5.

## 2. Definition of teleconnection indices

The prominent large-scale circulation features related to the SAT in the EAWM region are depicted by performing correlation analysis for the area-averaged SAT in the EAWM region (20°–50°N and 100°–140°E; green box in Fig. 2a) with the 500-hPa geopotential height ($Z_{500}$; shading in Fig. 2a). We use the following three steps to highlight the key regions responsible for the year-to-year variability of the SAT in the EAWM region (white contours in Fig. 2a):

- First, we repeat the correlation analysis for each of the grids in the EAWM region (221 grids in total). The output in the analysis is $r_1(\lambda,\phi,i)$, where $\lambda \in [0,357.5]$°E, $\phi \in [0,90.0]$°N and $i \in [1,221]$, and $r_1$ is the linear correlation coefficient between $Z_{500}$ and the SAT grid in the EAWM region.
- Second, to identify the regions accounting for a significant fraction of the SAT variability in the EAWM region, we set a threshold of 0.574 for $r_1$ (in magnitude; corresponding to 33.3% or one-third of the total variance). The thresh-

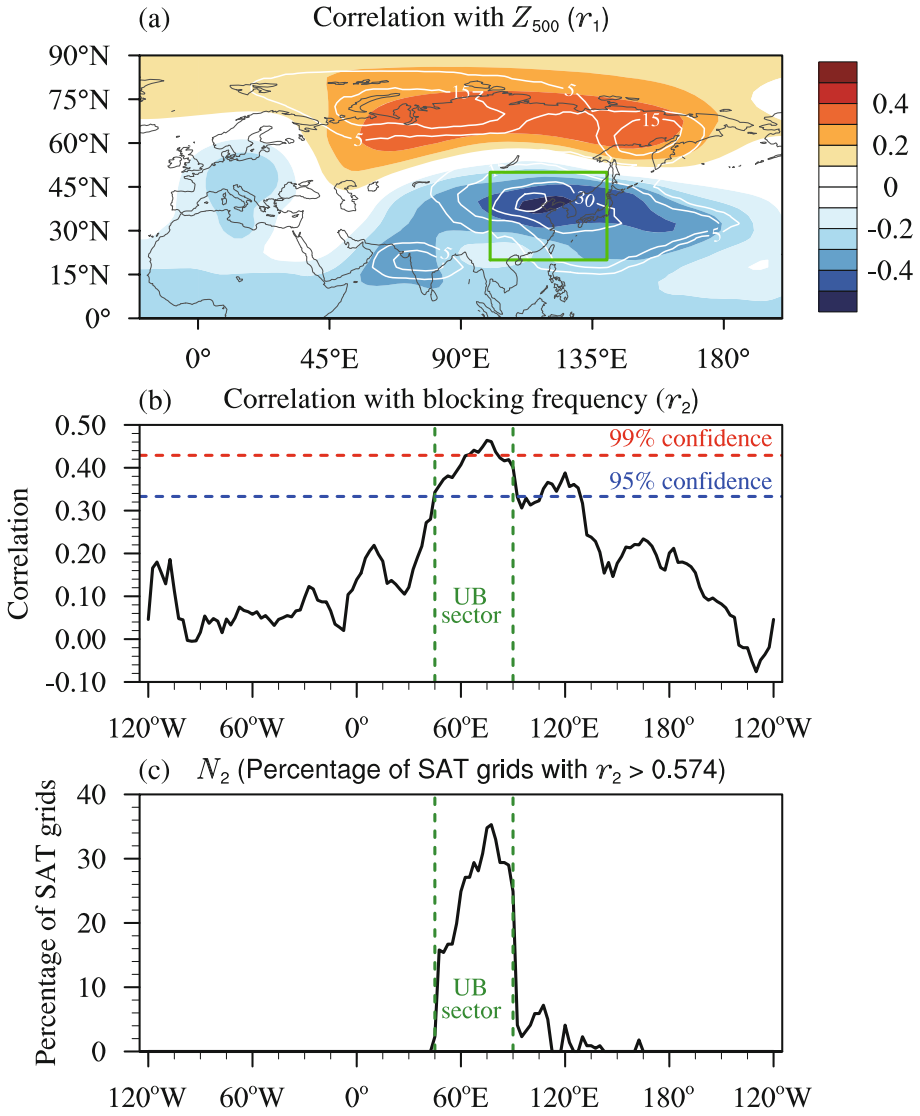


**Fig. 2.** Correlation between the area-averaged SAT in the EAWM region (green box) and (a) the $Z_{500}$ grids (shading), (b) the blocking frequency in the NH in the December–January–February period, where the percentage of SAT grids inside the box showing a linear correlation coefficient larger than 0.574 in magnitude with each of the $Z_{500}$ grids is denoted by the white contours in (a) , and that with blocking frequency is shown in (c).(see text for description)

old (0.574) is much greater than commonly used confidence levels (95% or 99%) with 65 degrees of freedom (where the length of study period is 66 years). The output in the analysis is $N_1(\lambda,\phi,i)$ (1 if exceeding the threshold and 0 otherwise).

• Third, at each $Z_{500}$ grid point $(\lambda,\phi)$ we count the percentage of SAT grids in the EAWM region with $r_1$ exceeding the threshold, where $N_1(\lambda,\phi) = [\sum_{i=1}^{221} N_1(\lambda,\phi,i)]/(221 \times 100)$ (%; white contours in Fig. 2a).

As shown in Fig. 2a, the year-to-year variability of the SAT over the EAWM region is teleconnected with both upstream and downstream signals over the extratropical region. Upstream of the East Asian continent is a tripole pattern, where a low region is centered over the European continent and the Mediterranean Sea (~ 15°E), while a high region is centered near the Ural Mountains (~ 60°E) and another low region can be found over western Siberia (~ 90°–100°E). This is analogous to the dominant UB pattern (Wang et al., 2010b; Cheung et al., 2012). A significant negative correlation is also found over the Arabian Sea (~ 20°N, 60°E), but further analysis reveals that this signal is significantly correlated with UB (figure not shown). On the other hand, downstream of the East Asian continent is a dipole pattern over the western North Pacific. This resembles the WP teleconnection pattern (Wallace and Gutzler, 1981). The above results suggest that UB and WP account for a significant fraction of the SAT variability in the EAWM region.

The $Z_{500}$ anomaly pattern resembles an inverted omega pattern (Yeh et al., 1962; Ding, 1994), suggesting that lower SAT in the EAWM region is related to the more frequent occurrence of blocking. The area-averaged SAT of the EAWM region is significantly correlated with the blocking frequency over 45°–90°E (the Urals sector) and 105°–130°E (the WP

sector; Fig. 2b). Note that the blocking frequency is defined in the same way as the algorithm listed in Cheung et al. (2015), which identifies the regions showing a reversal of $Z_{500}$ gradient over the midlatitudes for at least four consecutive days.

To identify the key blocking region accounting for a significant fraction of the SAT variability in the EAWM region, we follow the three steps that constructed the white contours in Fig. 2a. First, we correlate the blocking frequency at each longitude with each of the 221 SAT grids inside the EAWM region. The output of this correlation analysis is $r_2(\lambda, i)$, where $\lambda \in [0, 357.5]$°E and $i \in [1, 221]$. Second, we use $N_2(\lambda, i)$ to record whether the correlation exceeds the threshold (0.574 in magnitude), where $N_2(\lambda, i) = 1$ if exceeding this threshold and $N_2(\lambda, i) = 0$ otherwise. Third, for each longitude, we count the percentage of SAT grids in the EAWM region with $r_2$ exceeding the threshold, where $N_2(\lambda) = [\sum_{i=1}^{221} N_2(\lambda, i)]/(221 \times 100)$ (Fig. 2c).

As shown in Fig. 2c, more than 30% of the SAT grids are found to show a linear correlation coefficient larger than 0.574 in magnitude with the UB sector, but much less than 10% of the SAT grids have such a strong correlation with the WP blocking. Therefore, the Urals sector is the major blocking sector strongly linked to SAT variability in the EAWM region.

Accordingly, we deduce that a blocking pattern centered near the Urals and a north–south-oriented dipole over the western North Pacific are two large-scale atmospheric signals related to SAT variability in the EAWM region:

- Signal (1) can be represented by the UBI. This is defined as the first leading EOF pattern obtained from the covariance matrix of $Z_{500}$ enclosing the region (30°–80°N, 0°–120°E) (Fig. 3a). Each grid of the covariance matrix is weighed by $\cos\phi$. The definition is similar to that in Cheung et al. (2012), but a larger domain is chosen here in order to capture the tripole pattern in Fig. 2a. Unlike in Cheung et al. (2015), the area-averaged blocking frequency is not adopted here because the EOF pattern can be easily reproduced, and this EOF pattern is closely related to the UB frequency.
- Signal (2) is captured well by the western Pacific index (WPI). This is defined as the first leading EOF obtained from the correlation matrix of the $Z_{500}$ anomalies enclosing the region of (20°–80°N, 90°E–120°W), which resembles the WP pattern (Wallace and Gutzler, 1981; Cheung et al., 2015). Because the positive sign of the WPI represents a lower $Z_{500}$ over the high-latitude region of the North Pacific, its sign is reversed in Fig. 3b.

## 3. Distinct relationships with EAWM temperatures

After defining the two teleconnection patterns in Figs. 3a and b, their standardized principal component is correlated with the SAT field in order to illustrate their relationship with the EAWM temperatures. As shown in Figs. 3c and d, the

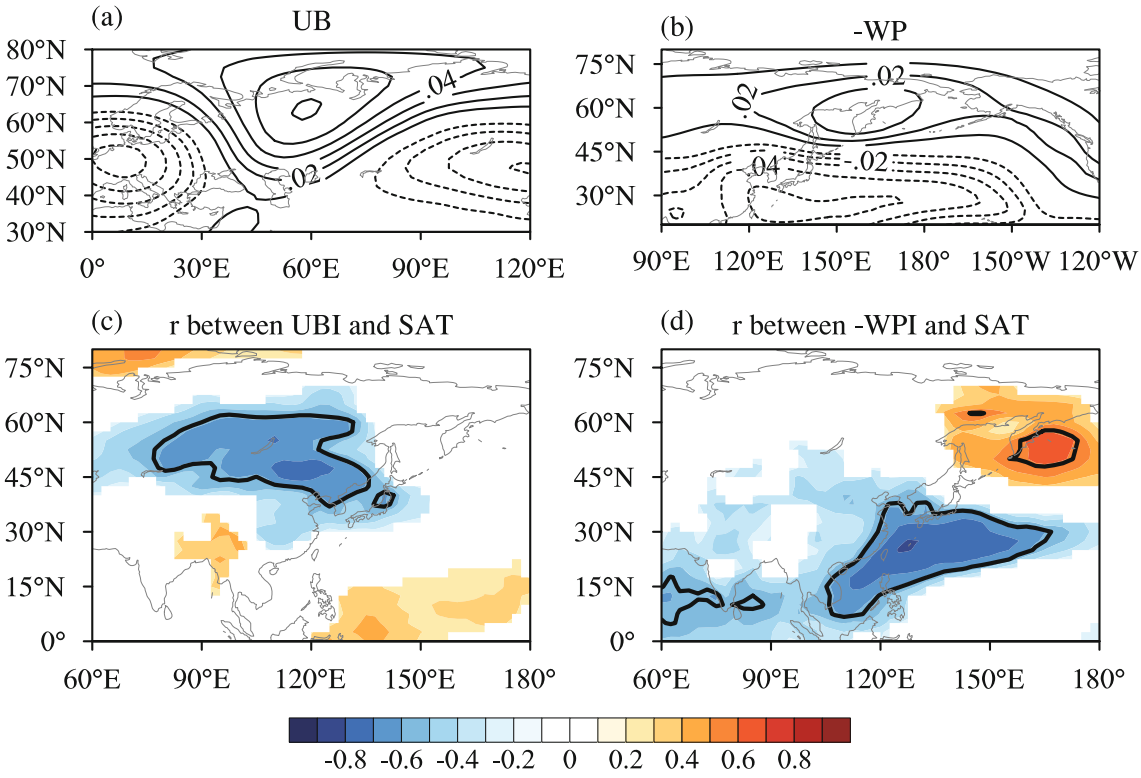


**Fig. 3.** Eigenvector of the (a) UB and (b) WP teleconnection pattern. Linear correlation coefficients between SAT and the principal component of (c) UB and (d) WP. In (c, d), only the regions significant at the 95% confidence level are shaded, and the values larger than 0.574 in magnitude (equivalent to one-third of the explained variance) are enclosed by thick contours.

two patterns are associated with two distinct temperature patterns in Asia. The UBI is significantly negatively correlated with the SAT over the midlatitude region in Asia (including Siberia, central and northern parts of China, Korea, and Japan), with the strongest negative correlation southeast of Lake Baikal (Fig. 3c). The WPI, on the other hand, is accompanied by a temperature dipole anomaly pattern over the Asia–Pacific region. In particular, the negative phase of the WPI is significantly negatively correlated with the SAT over the coastal region in East Asia and Southeast Asia, including southeastern China, South Korea, southern Japan, and Vietnam (Fig. 3d). In short, the UBI forms a very strong linkage with the SAT north of 40°N, whereas the WPI is strongly linked to the SAT south of 40°N in the EAWM region.

During the observational period, the interannual and interdecadal variations of the SAT in the EAWM region can be described mainly by two dominant modes (Wang et al., 2010a). Applying an EOF analysis to the covariance matrix of SAT in the EAWM region (0°–60°N, 100°–140°E), Wang et al. (2010a) called the first two EOFs the NTM and STM. The spatial patterns of the two temperature modes are given in Figs. 4a and b. Following their definitions, the two temperature modes were obtained using the ERA-40 datasets. Then, the principal component of the two SAT modes was obtained by projecting the two eigenvectors onto the NCEP data, where the climatological mean difference between the

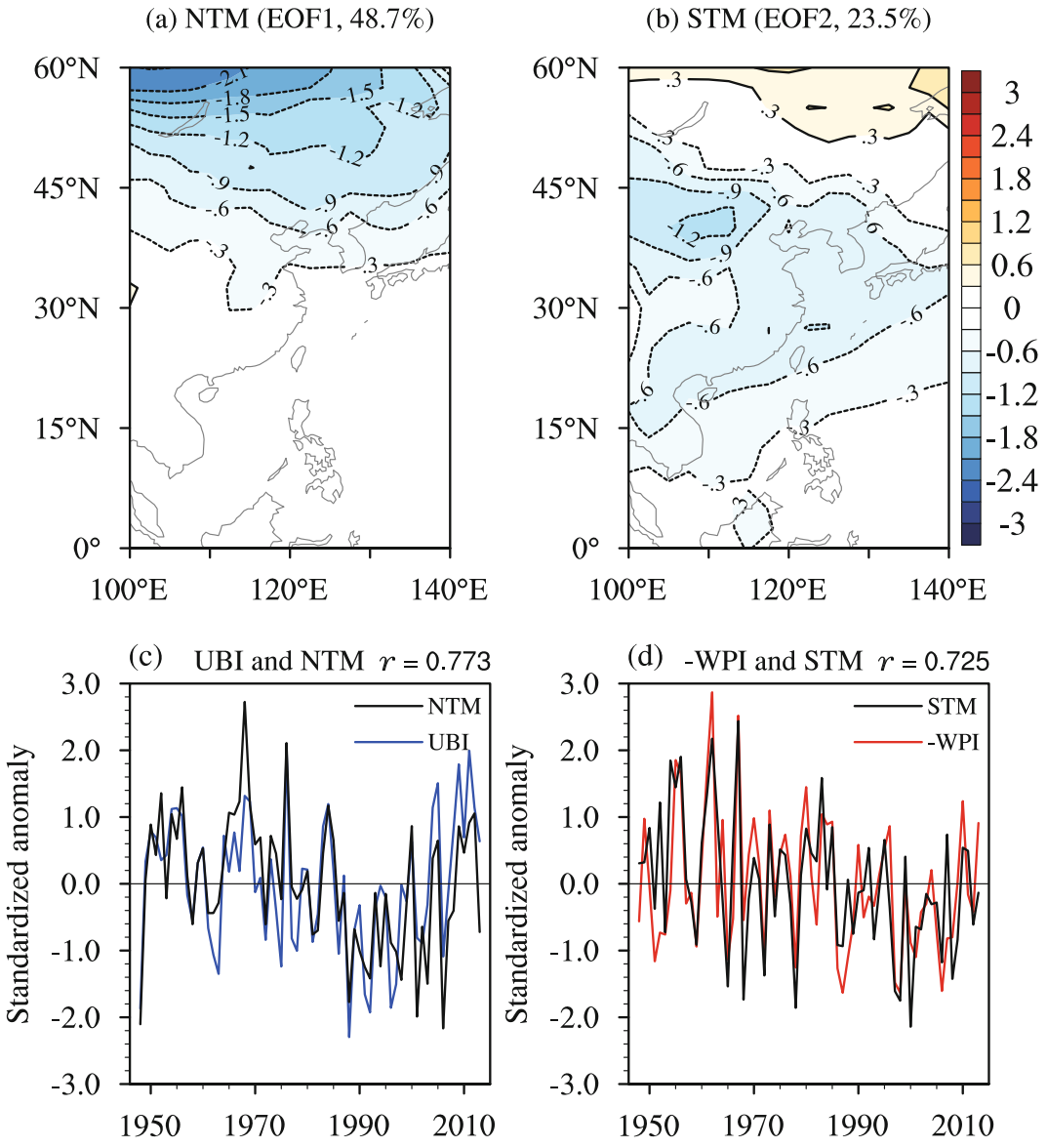


**Fig. 4.** (a, b) Spatial patterns of the first two leading EOF modes (EOF1 and EOF2) of SAT over the EAWM region (0°–60°N, 100°–140°E) using the ERA-40 dataset for the period 1957/58–2000/01: (a) NTM; (b) STM (units: °C) [redrawn from Wang et al. (2010a, Figs. 3a and c)]. (c, d) Standardized principal component of the NTM/STM (black line) and the time series of the UBI (blue line)/−WPI (red line). The linear correlation coefficient between the two time series is shown in the top-right.

NCEP and ERA-40 data was subtracted before the projection. The two modes account for 72% of the total variance, where the NTM (STM) explains well the SAT variability north (south) of 40°N. The region explained by the UBI (WPI) seems to coincide with that of the NTM (STM).

The UBI–NTM and WPI–STM relationships are revealed in Figs. 4c and d, where their year-to-year correlations are larger than 0.7 in magnitude and the explained variances are greater than 50%. Because the intensity of the EAWM has been found to have undergone a strong decadal variation in the late 1980s (e.g., Jhun and Lee, 2004; Wang et al., 2009b; Wang et al., 2010a), one might wonder if these relationships are still strong on interannual timescales. In other words, the relationship in Figs. 4c and d might be mainly due to the decadal variation. In this regard, we applied an 8-year high-pass (low-pass) Lanczos filter with 21 weights to extract the interannual (interdecadal) component of each time series in Figs. 4c and d (Fig. 5).

As can be seen in Figs. 5a and b, both the UBI–NTM and WPI–STM relationships still have a linear correlation coefficient of larger than 0.7 in magnitude on interannual timescales. On the other hand, NTM and STM undergo a decadal variation around 1986/87, where they change from a predominantly positive to negative phase (Fig. 5c–d). Correspondingly, the SAT in the EAWM region tends to be below normal before this period and above normal afterward (Lee et al., 2013). In the late 2000s, the two temperature modes become less negative due to some severe winters, which is consistent with the strengthening tendency of the EAWM after 2004/05 (Wang and Chen, 2014a). In comparison, both the UBI and WPI can capture the decadal change in the 1980s (dashed colored lines in Figs. 4c and d). The correlation between the interdecadal time series of the UBI and NTM is 0.887, and that between the WPI and STM is 0.883. Apparently, the UB and WP are two large-scale teleconnection patterns that can account for a significant fraction of SAT variability in different parts of the EAWM region on interannual and interdecadal timescales.

## 4. Representativeness of the UBI and WPI

To measure how well the UBI and WPI can capture SAT variability in the EAWM region compared to other EAWMIs

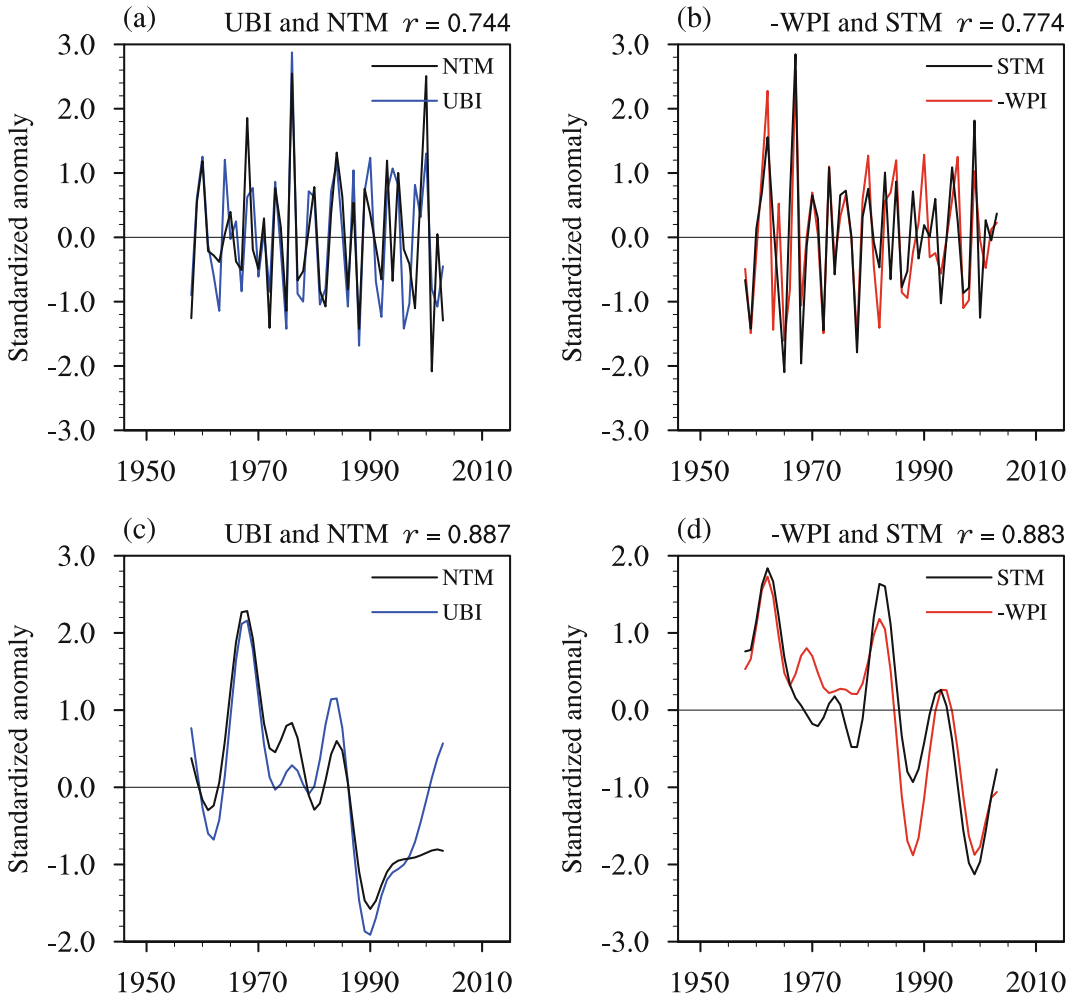


**Fig. 5.** As in Figs. 4c and d but for (a, b) the interannual component (<8 years) and (c, d) the interdecadal component (>8 years) of the time series.

and teleconnection patterns [Arctic Oscillation (AO), ENSO Niño3 index; Eurasian pattern (EU), Scandinavian pattern (SCAN)], all indices are correlated with the NTM and STM in Figs. 6a–d. The definition of all EAWMIs is given in Table 1, whereas the definitions of the teleconnection patterns are the same as those of the CPC/NOAA (http://www.cpc.ncep.noaa.gov/data/teledoc/telecontents.shtml). Because all climate indices on the CPC/NOAA website are available for 1950 onwards, the correlation analysis is confined to the period 1950/51–2013/14.

Among the 19 EAWMIs listed in Table 1, only five show a correlation of 0.50 or above in magnitude with the NTM in the entire study period (Fig. 6a). Two of them (WC14 and H15) are new indices, following the review of Wang and Chen (2010). They consider the meridional MSLP or $Z_{500}$ gradient over East Asia instead of solely the zonal gradient. The remaining three EAWMIs describe either the intensity of the Siberian high (G01) or the East Asian trough (S97 and CS99b). In contrast, only three EAWMIs have a correlation smaller than 0.50 in magnitude with the STM (Fig. 6b). These results are consistent with those of previous studies (e.g., Wang et al., 2010a; Wang and Chen, 2014a), where

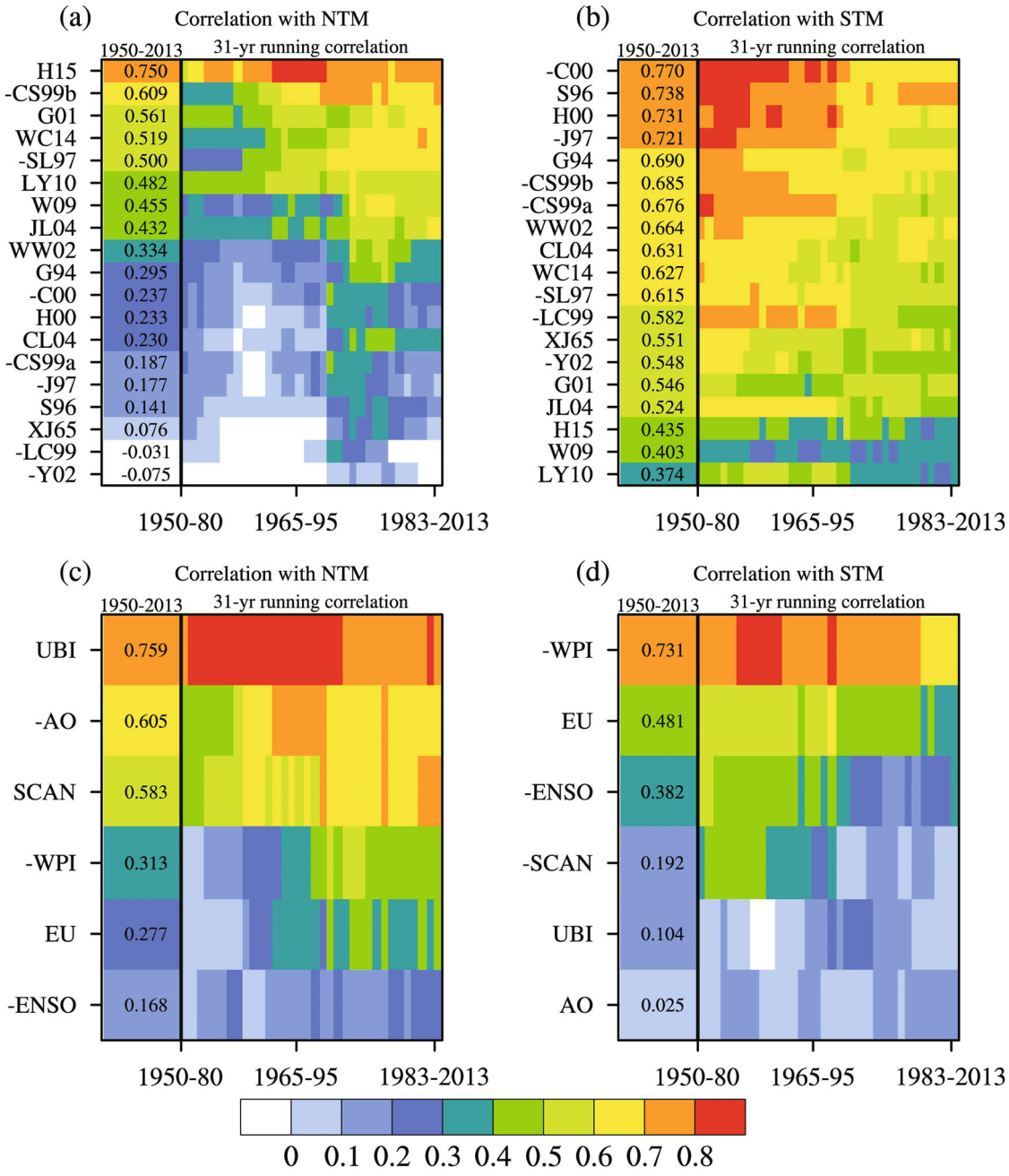


**Fig. 6.** Correlation between EAWMIs and the (a) NTM and (b) STM, where the first column of each plot shows the correlation throughout the entire study period, and the second column shows the 31-year running correlation. (c, d) As in (a, b) but for the correlation with teleconnection indices.

**Table 1.** List of EAWMIs. The EAWMIs considered in Wang and Chen's (2010) study are classified into four groups (EAWMI1 to EAWMI4) based on the parameter defining the index. The two remaining EAWMIs (WC14 and H15) have been defined recently.

| Type | Index | Definition | Publication |
|---|---|---|---|
| EAWMI1 | XJ65 | MSLP over (30°–40°N, 100°–120°E) minus MSLP over (30°–40°N, 130°–140°E) | Xu and Ji (1965) |
| EAWMI1 | G94 | Sum of MSLP over 10°–60°N at 110°E minus sum of MSLP over 10°–60°N at 160°E | Guo (1994) |
| EAWMI1 | S96 | Sum of MSLP anomaly over 20°–50°N at 110°E minus sum of MSLP anomaly over 20°–50°N at 160°E | Shi (1996) |
| EAWMI1 | G01 | MSLP over 40°–60°N and 70°–120°E | Gong et al. [2001] |
| EAWMI1 | WW02 | Sum of MSLP anomaly over 20°–70°N at 110°E minus sum of MSLP anomaly over 20°–70°N at 160°E | Wu and Wang (2002) |
| EAWMI1 | CL04 | MSLP over (30°–55°N, 100°–120°E) minus MSLP over (30°–55°N, 150°–170°E) | Chan and Li (2004) |
| EAWMI1 | W09 | Sum of MSLP anomaly over 40°–70°N at 110°E minus sum of MSLP anomaly over 40°–70°N at 160°E | Wang et al. (2009b) |
| EAWMI2 | J97 | $V_{1000}$ over (10°–30°N, 115°–130°E) | Ji et al. (1997) |
| EAWMI2 | LC99 | $V_{1000}$ over (7.5°–20°N, 107.5°–120°E) | Lu and Chan (1999) |
| EAWMI2 | CS99a | $V_{1000}$ over (15°–30°N, 115°–130°E) | Chen and Sun (1999) |
| EAWMI2 | C00 | $V$ at 10 m over (10°–25°N, 110°–130°E) and (25°–40°N, 120°–140°E) | Chen et al. (2000) |
| EAWMI2 | H00 | $-V$ at 10 m over (15°–40°N, 115°–130°E) | Hu et al. (2000) |
| EAWMI2 | Y02 | $U_{850}$ over (15°–30°N, 115°–130°E) | Yang et al. (2002) |
| EAWMI3 | SL97 | $Z_{500}$ over (35°–40°N, 110°–130°E) | Sun and Li (1997) |
| EAWMI3 | CS99b | $Z_{500}$ anomaly over (30°–45°N, 125°–145°E) | Cui and Sun (1999) |
| EAWMI4 | JL04 | $U_{300}$ over (27.5°–37.5°N, 110°–170°E) minus $U_{300}$ over (50°–60°N, 80°–140°E) | Jhun and Lee (2004) |
| EAWMI4 | LY10 | $(2\times U1-[U2+U3])/2$, where:<br>$U1=U_{200}$ over (30°–35°N, 90°–160°E);<br>$U2=U_{200}$ over (50°–60°N, 70°–140°E);<br>$U3=U_{200}$ over (30°–35°N, 90°–160°E). | Li and Yang (2010) |
| EAWMI* | WC14 | $(2\times \text{MSLP}-[\text{MSLP2}+\text{MSLP3}])/2$, where:<br>MSLP1 = MSLP anomaly over (40°–60°N, 70°–120°E);<br>MSLP2 = MSLP anomaly over (30°–50°N, 140°E–170°W);<br>MSLP3 = MSLP anomaly over (20°S–10°N, 110°–160°E). | Wang and Chen (2014a) |
| EAWMI* | H15 | $(4.9659\times \text{MSLP}_{H15}+5.0341\times Z_{H15})/10$, where:<br>$\text{MSLP}_{H15}=0.5\times(\text{MSLP1}+\text{MSLP2})$ and $Z_{H15}=0.5\times(Z1-Z2)$, in which:<br>MSLP1 = MSLP anomaly over (45°–65°N, 70°–130°E);<br>MSLP2 = 0.5× MSLP anomaly over (25°–45°N, 110°–120°E);<br>$Z_1=Z_{500}$ anomaly over (60°–72.5°N, 70°–110°E);<br>$Z_2=Z_{500}$ anomaly over (30°–42.5°N, 80°–120°E). | Hu et al. (2015) |

most of the EAWMIs were found to show a strong correlation with the STM but not the NTM.

As mentioned in Wang et al. (2010a), a cold NTM is characterized by a northwestward shift in the East Asian trough toward Lake Baikal (∼ 50°N, 110°E) and a northwestward shift in the Siberian high [which is located at (40°–65°N, 80°–120°E) in the climatology]. A cold STM, on the other hand, is related to a deepening of the East Asian trough and a stronger surface MSLP gradient between the Siberian high and the subtropical western North Pacific. Most of the EAWMIs listed in Table 1 belong to groups 1 and 2 (13 out of 19), where group 1 is defined by the zonal MSLP gradient between the Asian continent and the Pacific Ocean, and group 2 is defined by the lower tropospheric $V$ over the coastal region in East Asia. These EAWMIs describe mainly the large-scale circulation features south of 40°N. Accordingly, they tend to show a strong correlation with the STM that represents the SAT variability south of 40°N (Fig. 4b).

Compared to the EAWMIs and other well-known teleconnection indices, the UBI has the strongest correlation with the NTM, whereas the WPI has a correlation equally as strong (∼0.7) as that of four of the EAWMIs with the STM. Such strong year-to-year relationships are stable throughout the study period, as evidenced by slight changes in the 31-year running correlation. The above conclusion is still valid if we repeat the correlation analysis for the interannual and interdecadal component of the indices (same as Fig. 5), except that more EAWMIs show a correlation with the STM greater than 0.7 on the interannual timescales, and H15 shows a stronger correlation with the NTM (0.913) than the UBI (0.888) on the interdecadal timescales (figures not shown). Therefore, both the UBI and WPI are representative for measuring EAWM temperatures. Because many EAWMIs can represent the STM well, the remaining part of this section focuses on the NTM.

The UBI–NTM relationship is related to the linkage between UB and both the Siberian high and the East Asian trough. As can be inferred from Fig. 3a, the positive phase

of the UBI corresponds to stronger northerly geostrophic wind from the polar region towards western Siberia. This enhances the cold air intensity (i.e., negative SAT anomaly) over the climatological Siberian high region. Moreover, the stronger meridional-type circulation during the positive phase of the UBI tends to intensify the cyclonic flow over the East Asian continent, which can be deduced by the negative $Z_{500}$ anomaly over East Asia (Fig. 3a). This negative $Z_{500}$ anomaly pattern is analogous to the northwestward shift of the East Asian trough from the south of Japan towards the East Asian continent.

Compared to the UBI, SCAN shows a weaker correlation with the NTM throughout the study period. However, the 31-year moving correlation suggests that the SCAN–NTM relationship has become stronger in recent decades, which is comparable to the UBI–NTM relationship. Previous studies have also identified its impact on the EAWM (Bueh and Nakamura, 2007; Bueh et al., 2011; Sohn et al., 2011; Liu et al., 2014). The difference between SCAN and the UBI arises from their centers of action over Eurasia; those of SCAN are located at a higher latitude. The above results suggest that the large-scale circulations associated with the NTM are characterized by a quasi-stationary Rossby wave-train pattern recurring over Eurasia. This is also related to the location of UB. In future work, we will look to further explain the dynamic mechanisms responsible for the recurring position of blocking and the quasi-stationary Rossby wave train over Eurasia.

## 5. Summary and discussion

Based on recent advances in EAWM studies (e.g., Lee and Jhun, 2006; Wang et al., 2010a; Takaya and Nakamura, 2013; Kim et al., 2014; Liu et al., 2014; Hu et al., 2015; Leung and Zhou, 2015) and the results of this study, an EAWMI should be able to represent the following anomalous large-scale circulation features in order to capture the SAT variability in the majority of the EAWM region:

- The strength of the Siberian high, which is the cold-core system related to cold air activity over the EAWM region;
- The meridional-type circulation (or zonal index) over East Asia, which is related to the meridional displacement of the East Asian trough and the cold-air pathway in the EAWM region.

The former feature is captured well by any index enclosing the climatological Siberian high region (e.g., Hu et al., 2015). This is closely related to the teleconnection pattern centered near the Ural Mountains, which can be described by the UBI [Urals blocking pattern (Cheung et al., 2012)]. The latter feature is closely related to the deepening of the East Asian trough (Wang et al., 2009a; Leung and Zhou, 2015). This resembles the large-scale circulation features associated with the WPI (Lim and Kim, 2013; Takaya and Nakamura, 2013; Wang and Chen, 2014b). Therefore, variability in the EAWM can be explained well by the large-scale circulation features upstream and downstream of the EAWM region.

However, the SAT variability north and south of 40 °N in the EAWM region (NTM and STM) is quite different on interannual timescales. As a result, very few EAWMIs show an equally strong correlation with both the NTM and STM. Among the EAWMIs considered in this study, only CS99b (a trough index) shows a correlation above 0.60 with both the NTM and STM. We have also tried to use a linear combination of the UBI and WPI to represent the NTM and STM, and the optimization is $3 \times \mathrm{UBI} - 2 \times \mathrm{WPI}$. The correlation between this linear combination and the NTM (STM) is 0.614 (0.626), which is close to that of CS99b. In other words, a unified and representative EAWMI (say, with an explained variance larger than 50% in the entire EAWM region) is not easy to establish. One possible way is to consider the latitude and longitude dependence of SAT on the two important EAWM circulation features mentioned above (i.e., EAWMI is a function of latitude and longitude).

To improve the seasonal forecasting of temperature anomalies in the EAWM and to project future changes in the EAWM, more in-depth analyses should be carried out to explore the underlying dynamics regarding the large-scale teleconnections related to the EAWM, such as the UB and WP. The WP is related to ENSO, which has been discussed extensively in previous studies (e.g., Li, 1990; Wang et al., 2000; Zhou et al., 2007; Wang et al., 2008; Takaya and Nakamura, 2013; Chen et al., 2014). On the other hand, UB has been studied less extensively.

On synoptic timescales, UB is an important dynamic precursor of severe cold-air outbreaks in the EAWM. The occurrence of UB strengthens cold-air advection from the polar region to western Siberia. This enhances the Siberian high and subsequent cold-air outbreaks in the EAWM (Tao, 1957; Takaya and Nakamura, 2005; Lu and Chang, 2009; Zhou et al., 2009; Cheung et al., 2013). On seasonal timescales, when UB occurs frequently in a particular winter, the Siberian high intensity tends to be higher than normal. Because of the close linkage between the Siberian high intensity and the NTM, the temperature tends to be lower in the northern part of the EAWM (Wang et al., 2010b; Chang and Lu, 2012; Cheung et al., 2012). Moreover, the occurrence of UB is also characterized by a stronger meridional-type flow over East Asia. The more frequent occurrence of UB partly enhances the southward intrusion of cold air into the southern part of the EAWM. This potentially causes more frequent cold extremes in the EAWM, as in Hong Kong (Cheung et al., 2015). Therefore, the dynamics of UB should be investigated in depth in order to improve the understanding of the EAWM on different timescales. In addition to the major dynamic factors that lead to the occurrence of UB, we should understand the factors related to the recurring location of UB.

***Acknowledgements.*** The authors greatly appreciate the valuable comments provided by the two anonymous reviewers, which helped improve the clarity of the manuscript. The work described in this paper was supported by Shenzhen Research Project (Grant No. GJHS20120820144245169), and the French/Hong Kong Joint Research Project (No. F-HK002/12T).

## REFERENCES


Bueh, C., and H. Nakamura, 2007: Scandinavian pattern and its climatic impact. *Quart. J. Roy. Meteor. Soc.*, **133**, 2117–2131, doi: 10.1002/qj.173.

Bueh, C., N. Shi, and Z. W. Xie, 2011: Large-scale circulation anomalies associated with persistent low temperature over southern China in January 2008. *Atmos. Sci. Lett*., **12**, 273–280, doi: 10.1002/asl.333.

Chan, J. C. L., and C. Y. Li, 2004: The East Asian winter monsoon. *East Asian Monsoon*, C.-P. Chang, Ed., World Scientific Publishing Co. Pet. Ltd., 54–106.

Chang, C.-P., and K. M. W. Lau, 1980: Northeasterly cold surges and near-equatorial disturbances over the winter MONEX area during December 1974. Part II: Planetary-scale aspects. *Mon. Wea. Rev.*, **108**, 298–312.

Chang, C.-P., and M.-M. Lu, 2012: Intraseasonal predictability of Siberian high and East Asian winter monsoon and its interdecadal variability. *J. Climate*, **25**, 1773–1778, doi: 10.1175/JCLI-D-11-00500.1.

Chen, J., and S. Q. Sun, 1999: Eastern Asian winter monsoon anomaly and variation of global circulation Part I: A comparison study on strong and weak winter monsoon. *Chinese J. Atmos. Sci.*, **23**, 101–111. (in Chinese).

Chen, W., H.-F. Graf, and R. H. Huang, 2000: The interannual variability of East Asian winter monsoon and its relation to the summer monsoon. *Adv. Atmos. Sci*., **17**, 48–60, doi: 10.1007/s00376-000-0042-5.

Chen, Z., R. G. Wu, and W. Chen, 2014: Distinguishing interannual variations of the northern and southern modes of the east Asian winter monsoon. *J. Climate*, **27**, 835–851, doi: 10.1175/JCLI-D-13-00314.1.

Cheung, H. H. N., and W. Zhou, 2015: Implications of Ural blocking for East Asian winter climate in CMIP5 GCMs. Part I: Biases in the historical scenario. *J. Climate*, **28**, 2203–2216, doi: 10.1175/JCLI-D-14-00308.1.

Cheung, H. N., W. Zhou, H. Y. Mok, and M. C. Wu, 2012: Relationship between Ural–Siberian blocking and the East Asian winter monsoon in relation to the Arctic oscillation and the El Niño–southern oscillation. *J. Climate*, **25**, 4242–4257, doi: 10.1175/JCLI-D-11-00225.1.

Cheung, H. N., W. Zhou, Y. P. Shao, W. Chen, H. Y. Mok, and M. C. Wu, 2013: Observational climatology and characteristics of wintertime atmospheric blocking over Ural–Siberia. *Climate Dyn.*, **41**, 63–79.

Cheung, H. H. N., W. Zhou, S. M. Lee, and H. W. Tong, 2015: Interannual and interdecadal variability of the number of cold days in Hong Kong and their relationship with large-scale circulation. *Mon. Wea. Rev.*, **143**, 1438–1454, doi: 10.1175/MWR-D-14-00335.1.

Cui, X. P., and Z. B. Sun, 1999: East Asian winter monsoon index and its variation analysis. *Journal of Nanjing Institute of Meteorology*, **22**, 321–325. (in Chinese).

Ding, Y. H., 1994: *Monsoon over China*. Kluwer Academic Publishers, 420 pp.

Gong, D. Y., S. W. Wang, and J. H. Zhu, 2001: East Asian winter monsoon and Arctic oscillation. *Geophys. Res. Lett.*, **28**, 2073–2076.

Guo, Q. W., 1994: Relationship between the variations of East Asian winter monsoon and temperature anomalies in China. *Quarterly Journal of Applied Meteorology*, **5**, 218–225. (in Chinese).

Hsu, H.-H., and J. M. Wallace, 1985: Vertical structure of wintertime teleconnection patterns. *J. Atmos. Sci.*, **42**, 1693–1710.

Hu, C. D., S. Yang, and Q. G. Wu, 2015: An optimal index for measuring the effect of East Asian winter monsoon on China winter temperature. *Climate Dyn.*, **45**, 2751–2589, doi: 10.1007/s00382-015-2493-5.

Hu, Z.-Z., L. Bengtsson, and K. Arpe, 2000: Impact of global warming on the Asian winter monsoon in a coupled GCM. *J. Geophys. Res.*, **105**, 4607–4624, doi: 10.1029/1999JD901031.

Jhun, J. G., and E. J. Lee, 2004: A new East Asian winter monsoon index and associated characteristics of the winter monsoon. *J. Climate*, **17**, 711–726, doi: 10.1175/1520-0442(2004)017<0711:ANEAWM>2.0.CO;2.

Ji, L. R., S. Q. Sun, K. Arpe, and L. Bengtsson, 1997: Model study on the interannual variability of Asian winter monsoon and its influence. *Adv. Atmos. Sci.*, **14**, 1–22, doi: 10.1007/s00376-997-0039-4.

Joung, C. H., and M. H. Hitchman, 1982: On the role of successive downstream development in East Asian polar air outbreaks. *Mon. Wea. Rev.*, **110**, 1224–1237.

Kim, Y., K. Y. Kim, and S. Park, 2014: Seasonal scale variability of the East Asian winter monsoon and the development of a two-dimensional monsoon index. *Climate Dyn.*, **42**, 2159–2172, doi: 10.1007/s00382-013-1724-x.

Lau, N.-C., and K.-M. Lau, 1984: The structure and energetics of midlatitude disturbances accompanying cold-air outbreaks over East Asia. *Mon. Wea. Rev.*, **112**, 1309–1327, doi: 10.1175/1520-0493(1984)112<1309:TSAEOM>2.0.CO;2.

Lee, H. S., and J. G. Jhun, 2006: Two types of the Asian continental blocking and their relation to the east Asian monsoon during the boreal winter. *Geophys. Res. Lett.*, **33**, L22707, doi: 10.1029/2006GL027948.

Lee, S.-S., S.-H. Kim, J.-G. Jhun, K.-J. Ha, and Y.-W. Seo, 2013: Robust warming over East Asia during the boreal winter monsoon and its possible causes. *Environ. Res. Lett*., **8**, 034001, doi: 10.1088/1748-9326/8/3/034001.

Leung, M. Y.-T., and W. Zhou, 2015: Variation of circulation and East Asian climate associated with anomalous strength and displacement of the East Asian trough. *Climate Dyn.*, **45**, 2731–2732, doi: 10.1007/s00382-015-2504-6.

Li, C. Y., 1990: Interaction between anomalous winter monsoon in East Asia and El Niño events. *Adv. Atmos. Sci.,* **7**, 36–46, doi: 10.1007/BF02919166.

Li, Y. Q., and S. Yang, 2010: A dynamical index for the East Asian winter monsoon. *J. Climate*, **23**, 4255–4262, doi: 10.1175/2010JCLI3375.1.

Lim, Y. K., and H. D. Kim, 2013: Impact of the dominant large-scale teleconnections on winter temperature variability over East Asia. *J. Geophys. Res.*, **118**, 7835–7848, doi: 10.1002/jgrd.50462.

Lim, Y.-K., and H.-D. Kim, 2015: Comparison of the impact of the Arctic Oscillation and Eurasian teleconnection on interannual variation in East Asian winter temperatures and monsoon. *Theor. Appl. Climatol.*, 1–13, doi: 10.1007/s00704-015-1418-x.

Liu, Y. Y., L. Wang, W. Zhou, and W. Chen, 2014: Three Eurasian teleconnection patterns: Spatial structures, temporal variability, and associated winter climate anomalies. *Climate Dyn*., **42**, 2817–2839, doi: 10.1007/s00382-014-2163-z.

Lu, E., and J. C. L. Chan, 1999: A unified monsoon index for South China. *J. Climate*, **12**, 2375–2385, doi: 10.1175/1520-

0442(1999)012<2375:AUMIFS>2.0.CO;2.

Lu, M. M., and C.-P. Chang, 2009: Unusual late-season cold surges during the 2005 Asian winter monsoon: Roles of Atlantic blocking and the central Asian anticyclone. *J. Climate*, **22**, 5205–5217, doi: 10.1175/2009JCLI2935.1.

Shi, N., 1996: Features of the East Asian winter monsoon intensity on multiple time scale in recent 40 years and their relation to climate. *Journal of Applied Meteorological Science*, **7**, 175–182. (in Chinese).

Sohn, S.-J., C.-Y. Tam, and C.-K. Park, 2011: Leading modes of East Asian winter climate variability and their predictability: An assessment of the APCC multi-model ensemble. *J. Meteor. Soc. Japan*, **89**, 455–474, doi: 10.2151/jmsj.2011-504.

Song, J., C. Y. Li, and W. Zhou, 2014: High and low latitude types of the downstream influences of the North Atlantic Oscillation. *Climate Dyn.*, **42**, 1097–1111, doi: 10.1007/s00382-013-1844-3.

Sun, B.-M., and C.-Y. Li, 1997: Relationship between the disturbances of East Asian trough and tropical convective activity in boreal winter. *Chinese Science Bulletin*, **42**, 500–504. (in Chinese).

Takaya, K., and H. Nakamura, 2005: Mechanisms of intraseasonal amplification of the cold Siberian high. *J. Atmos. Sci.*, **62**, 4423–4440, doi: 10.1175/JAS3629.1.

Takaya, K., and H. Nakamura, 2013: Interannual variability of the East Asian winter monsoon and related modulations of the planetary waves. *J. Climate*, **26**, 9445–9461, doi: 10.1175/JCLI-D-12-00842.1.

Tao, S. Y., 1957: A study of activities of cold airs in East Asian winter. *Handbook of Short-Term Forecast*, China Meteorological Administration, Ed., Meteorology Press, 60–92.

Wallace, J. M., and D. S. Gutzler, 1981: Teleconnections in the geopotential height field during the northern hemisphere winter. *Mon. Wea. Rev.*, **109**, 784–812.

Wang, B., R. G. Wu, and X. H. Fu, 2000: Pacific–East Asian teleconnection: how does ENSO affect East Asian climate? *J. Climate*, **13**, 1517–1536, doi: 10.1175/1520-0442(2000)013<1517:PEATHD>2.0.CO;2.

Wang, B., Z. W. Wu, C.-P. Chang, J. Liu, J. P. Li, and T. J. Zhou, 2010a: Another look at interannual-to-interdecadal variations of the east Asian winter monsoon: The northern and southern temperature modes. *J. Climate*, **23**, 1495–1512, doi: 10.1175/2009JCLI3243.1.

Wang, L., and W. Chen, 2010: How well do existing indices measure the strength of the East Asian winter monsoon? *Adv. Atmos. Sci.*, **27**, 855–870, doi: 10.1007/s00376-009-9094-3.

Wang, L., and W. Chen, 2014a: The East Asian winter monsoon: re-amplification in the mid-2000s. *Chinese Science Bulletin*, **59**, 430–436, doi: 10.1007/s11434-013-0029-0.

Wang, L., and W. Chen, 2014b: An intensity index for the East Asian winter monsoon. *J. Climate*, **27**, 2361–2374, doi: 10.1175/JCLI-D-13-00086.1.

Wang, L., W. Chen, and R. H. Huang, 2008: Interdecadal modulation of PDO on the impact of ENSO on the east Asian winter monsoon. *Geophys. Res. Lett.*, **35**, doi: 10.1029/2008GL035287.

Wang, L., W. Chen, W. Zhou, and R. H. Huang, 2009a: Interannual variations of East Asian trough axis at 500 hPa and its association with the East Asian winter monsoon pathway. *J. Climate*, **22**, 600–614, doi: 10.1175/2008JCLI2295.1.

Wang, L., R. H. Huang, L. Gu, W. Chen, and L. H. Kang, 2009b: Interdecadal variations of the East Asian winter monsoon and their association with quasi-stationary planetary wave activity. *J. Climate*, **22**, 4860–4872, doi: 10.1175/2009JCLI2973.1.

Wang, L., W. Chen, W. Zhou, J. C. L. Chan, D. Barriopedro, and R. H. Huang, 2010b: Effect of the climate shift around mid 1970s on the relationship between wintertime Ural blocking circulation and East Asian climate. *Int. J. Climatol.*, **30**, 153–158, doi: 10.1002/joc.1876.

Wu, B. Y., and J. Wang, 2002: Winter Arctic oscillation, Siberian high and East Asian winter monsoon. *Geophys. Res. Lett.*, **29**, 1897, doi: 10.1029/2002GL015373.

Xu, S. Y., and J. J. Ji, 1965: The climate and weather features during the outbreak period of China's winter monsoon. *Geographical Symposium*, **9**, 85–101. (in Chinese).

Yang, S., K.-M. Lau, and K.-M. Kim, 2002: Variations of the East Asian jet stream and Asian-Pacific-American winter climate anomalies. *J. Climate*, **15**, 306–325, doi: 10.1175/1520-0442(2002)015<0306:VOTEAJ>2.0.CO;2.

Yeh, T.-C., S. Y. Tao, and B. Z. Zhu, 1962: *Studies on the Blocking Situation in the Northern Hemisphere in Winter*. Science Press, 130 pp. (in Chinese).

Zhou, W., X. Wang, T. J. Zhou, C. Li, and J. C. L. Chan, 2007: Interdecadal variability of the relationship between the East Asian winter monsoon and ENSO. *Meteor. Atmos. Phys.*, **98**, 283–293, doi: 10.1007/s00703-007-0263-6.

Zhou, W., J. C. L. Chan, W. Chen, J. Ling, J. G. Pinto, and Y. P. Shao, 2009: Synoptic-scale controls of persistent low temperature and icy weather over southern China in January 2008. *Mon. Wea. Rev.*, **137**, 3978–3991, doi: 10.1175/2009MWR2952.1.